*quantum beam science*

MDPI

*Article*

# Chromatic Change in Copper Oxide Layers Irradiated with Low Energy Ions

**Takuya Kobayashi [1], Fumitaka Nishiyama [2] and Katsumi Takahiro [1,*]**

[1] Faculty of Materials Science and Engineering, Kyoto Institute of Technology, Matsugasaki, Sakyo, Kyoto 606-8585, Japan; m0672011@edu.kit.ac.jp
[2] Research Institute of Nanodevice and Bio Systems, Hiroshima University, Kagamiyama 1-4-1, Higashi-Hiroshima, Hiroshima 739-8527, Japan; fnishi@hiroshima-u.ac.jp
* Correspondence: takahiro@kit.ac.jp

**Abstract:** The color of a thin copper oxide layer formed on a copper plate was transformed from reddish-brown into dark blue-purple by irradiation with 5 keV $Ar^+$ ions to a fluence as low as $1 \times 10^{15}$ $Ar^+$ $cm^{-2}$. In the unirradiated copper oxide layer, the copper valence state of $Cu^{2+}$ and $Cu^+$ and/or $Cu^0$ was included as indicated by the presence of a shake-up satellite line in a photoemission spectrum. While for the irradiated one, the satellite line decreased in intensity, indicating that irradiation resulted in the reduction from $Cu^{2+}$ to $Cu^+$ and/or $Cu^0$. Furthermore, nuclear reaction analysis using a $^{16}O(d, p)^{17}O$ reaction with 0.85 MeV deuterons revealed a significant loss of oxygen ($5 \times 10^{15}$ O atoms $cm^{-2}$) in the irradiated layer. Thus, the chromatic change observed in the present work originated in the irradiation-induced reduction of a copper oxide.

**Keywords:** ion beam; copper oxide; chromatic change; photoemission spectrum; beam viewer

check for updates

**Citation:** Kobayashi, T.; Nishiyama, F.; Takahiro, K. Chromatic Change in Copper Oxide Layers Irradiated with Low Energy Ions. *Quantum Beam Sci.* **2021**, *5*, 7. https://doi.org/10.3390/qubs5010007

Academic Editor: Akihiro Iwase

Received: 2 February 2021
Accepted: 9 March 2021
Published: 10 March 2021

**Publisher's Note:** MDPI stays neutral with regard to jurisdictional claims in published maps and institutional affiliations.

**Copyright:** © 2021 by the authors. Licensee MDPI, Basel, Switzerland. This article is an open access article distributed under the terms and conditions of the Creative Commons Attribution (CC BY) license (https://creativecommons.org/licenses/by/4.0/).

## 1. Introduction

On ion beam experiments including materials analysis and modification with ion beams, a beam monitoring system is installed in the sample chamber to monitor the beam position and uniformity in the beam spot. Most of the beam monitor consists of a fluorescent plate, enabling real time visualization of a beam spot on the plate. A $SiO_2$ plate, for example, has been used for beam monitoring because of strong emission [1–5] in the visible range when irradiated with MeV-ion beams. A Cr-doped $Al_2O_3$ (e.g., AF995R, Desmarquest) is also suitable for beam profiling [6,7] for ion beams with energies larger than several hundred keV. The aforementioned materials are insulators and therefore electric charging takes places on the fluorescent plate irradiated with ion beams, resulting in deflection of ion beams in the vicinity of the fluorescent plate if their acceleration voltage is comparable to the charged potential of a few tens kilovolts [8]. This means that the fluorescent point would be different from the real position, and further the fluorescent point would not appear at all in the case of low energy ion beams with <10 keV. In addition to the fluorescent materials, phosphors such as ZnS based materials [9–11], which have been widely used for screens of a cathode-ray tube, are applicable to beam monitoring. Other candidates of inorganic luminescent materials can be found in the literature [12]. Powders of such materials, mixed with a conducting paste and deposited onto a conducting plate, are a candidate for ion beam monitoring materials. However, such powders cost very high, but their lifetimes are very short because radiation damage causes degradation of light-emitting efficiency. It is, therefore, not easy to view a beam spot of a low energy ion beam with energy of several keV on real-time.

On the other hand, non-real time beam monitoring can be conducted by the color change of materials irradiated with ion beams. A polyimide film is, for example, widely used to check both the position and uniformity of an ion beam, because blackening due to graphitization [13–15] occurs when the film is irradiated with ion beams. A polyimide

film is, however, non-conducting and is inapplicable to the beam viewer for low energy ion beams with energies of several keV. The favorable beam viewer for low energy ion beams should be composed of electrically conducting materials. A metallic copper plate, even if a thin upper layer of copper oxide is present, is a good conducting material. The color of the copper plate covered with thin oxide is reddish-brown, largely different from polished metallic copper. The present authors made an attempt to fabricate a beam viewer in which the appearance of a beam spot turns shiny due to removal of the oxide layer by physical sputtering. In the irradiation apparatus with base pressure of $2 \times 10^{-4}$ Pa, the shiny beam spot could be clearly recognized after irradiation with 5 keV $Ar^+$ ions to a fluence of $1 \times 10^{15}$ $Ar^+$ $cm^{-2}$. Surprisingly, in the other irradiation equipment with base pressure of $2 \times 10^{-6}$ Pa, the color of the beam spot turned dark blue-purple after irradiation under the same conditions above. In the present work, the chromatic change observed in the irradiation equipment with such a high vacuum is examined to fabricate a new type of beam viewer for low energy ion beams.

## 2. Materials and Methods

Oxygen-free copper plates of $10 \times 10 \times 1$ $mm^3$ (purity 99.99%) were supplied from NILACO, Tokyo, Japan. The Cu plate was put on a laboratory hot plate setting to 473 K in ambient air for 2 min to form the Cu oxide layer. The maximum temperature measured on the surface with chromel-alumel thermocouple was 440 K, somewhat lower than the setting temperature of 473 K, as recorded in Figure 1. The color of heat-treated Cu plate was reddish-brown. The samples were irradiated with 5 keV-$Ar^+$ ions up to a fluence of $1 \times 10^{15}$ $cm^{-2}$ using a 5 kV-ion gun installed in a vacuum chamber with a base pressure of $2 \times 10^{-6}$ Pa. The ion incidence was normal with respect to the sample surface.

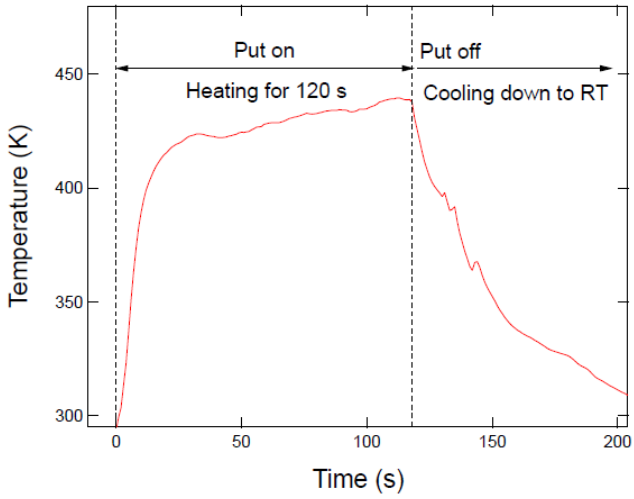


**Figure 1.** Temperature measured on the sample surface with chromel-alumel thermocouple during oxidation.

X-ray photoelectron spectroscopy (XPS) using Mg Kα radiation ($h\nu$ = 1253.6 eV) was performed with a JEOL 9010 X-ray photoelectron spectrometer (JEOL, Tokyo, Japan) to analyze chemical states of Cu before and after the irradiation. The XPS analysis was carried out immediately after the irradiation to avoid the change in chemical states upon the ambient air exposure. Rutherford backscattering spectrometry (RBS) and nuclear reaction analysis (NRA) using the $^{16}O(d, p)^{17}O$ reaction were conducted for chemical composition analysis with 2 MeV He ions and 0.85 MeV deuterons, respectively, produced from the Van de Graaff accelerator of Hiroshima University. The standard sample for the NRA was a $SiO_2$ layer formed on a Si wafer ($SiO_2$/Si), which contains $5.8 \times 10^{17}$ O atoms·$cm^{-2}$ determined by RBS.

## 3. Results and Discussion

Figure 2a shows a photograph of the sample surface irradiated with $Ar^+$ ions to a fluence of $1 \times 10^{15}$ $cm^{-2}$ using a 5 kV ion gun. The color of the sample changed from reddish brown to dark blue-purple at an irradiation spot. This darkening was visible through a viewing port, and started at the fluence as low as $10^{14}$ $cm^{-2}$. On the sample surface irradiated to a fluence of $10^{14}$ $cm^{-2}$, the color of the edge at the beam spot was not clear as can be seen in Figure 2b, indicating that the border between irradiated and unirradiated areas was not so abrupt. Thus, the uniformity of a beam intensity inside the beam spot could be estimated by the uniformity of color. The minimum fluence to recognize the beam spot with naked eyes will be examined for further discussion of the sensitivity and applicability of the chromatic change for a beam viewer.

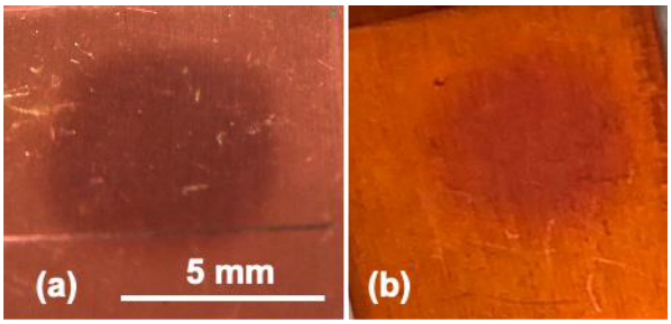


**Figure 2.** Photographs of the surface of samples irradiated with 5 keV-$Ar^+$ ions to fluences of $1 \times 10^{15}$ $cm^{-2}$ (**a**) and $1 \times 10^{14}$ $cm^{-2}$ (**b**). The photographs were taken after removing the samples from the vacuum chamber.

The mechanism of the observed chromatic change was discussed below, along with RBS, NRA, and XPS data. Figure 3 shows the backscattering spectrum of the Cu oxide layer formed on a Cu plate before irradiation. The chemical composition and thickness of the oxide layer was estimated to be $CuO_{0.4}$ and $1.9 \times 10^{17}$ $CuO_{0.4}$ $cm^{-2}$, respectively, by fitting a simulation spectrum to experimental data, where the program SIMNRA 6.06 [16] was used to obtain the simulation spectrum. The thickness of $1.9 \times 10^{17}$ $CuO_{0.4}$ $cm^{-2}$ can be converted into 38 nm, much larger than the ion projected range of 5 nm predicted by the SRIM simulation [17], assuming the atomic density to be $5 \times 10^{22}$ $CuO_{0.4}$ $cm^{-3}$. The chemical composition $CuO_{0.4}$ indicates that the oxide layer contains the mixture of metallic copper and copper oxides.

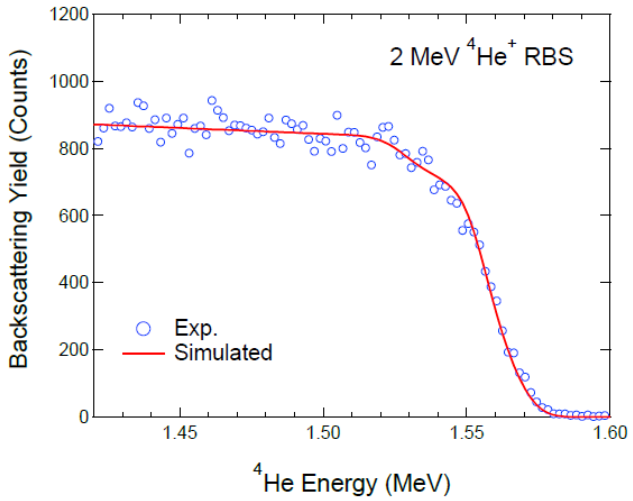


**Figure 3.** RBS spectrum of the sample before irradiation (blue open circles). A simulated spectrum (red solid line) is also shown.

Figure 4 presents the NRA spectra of the sample with and without irradiation. Peaks located around channel number of 260 correspond to protons emitted by the $^{16}O(d, p)^{17}O$ reaction. The peak intensities are $(2.15 \pm 0.05) \times 10^3$ and $(2.01 \pm 0.04) \times 10^3$ counts for the unirradiated and irradiated samples, respectively. The oxygen content in the irradiated sample was determined to be $(7.1 \pm 0.2) \times 10^{16}$ O atoms·cm$^{-2}$ by the $SiO_2$/Si standard sample, smaller by 6% than that in the unirradiated sample ($(7.6 \pm 0.2) \times 10^{16}$ O atoms·cm$^{-2}$). Thus, oxygen atoms were found to be released from the $CuO_{0.4}$ layer by the irradiation with 5 keV-Ar$^+$ ions to a fluence of $1 \times 10^{15}$ cm$^{-2}$. The SRIM simulation [17] predicts the sputtering yield of O in $CuO_{0.4}$ to be 4.9 O atoms·ion$^{-1}$, which means that the sputtered O atoms will be approximately $5 \times 10^{15}$ O atoms·cm$^{-2}$, corresponding to a difference in the oxygen contents between the unirradiated and irradiated samples. The NRA results and the SRIM calculation suggest that the release of O atoms originates in physical sputtering. In the sputtering process of $CuO_{0.4}$ bombarded with 5 keV-Ar$^+$ ions, approximately $1.4 \times 10^{15}$ Cu atoms·cm$^{-2}$ as calculated by the SRIM will be lost, leading to the change in chemical composition from $CuO_{0.4}$ to $CuO_{0.38}$ in the layer.

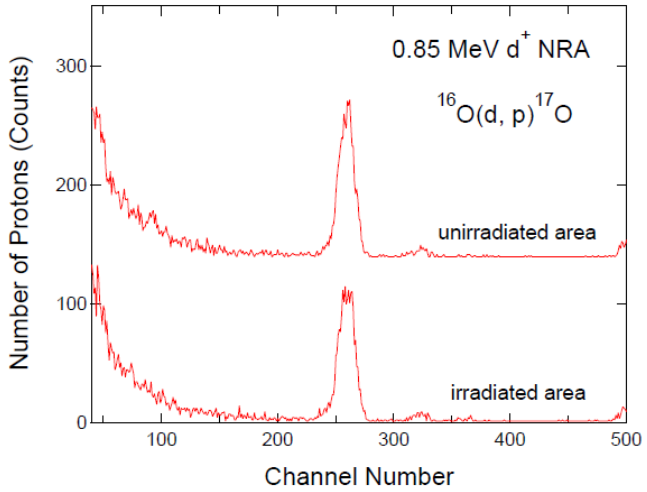


**Figure 4.** Nuclear reaction analysis (NRA) spectra of the unirradiated and irradiated areas in the sample irradiated with 5 keV-Ar+ ions to a fluence of $1 \times 10^{15}$ cm$^{-2}$.

Figure 5 shows XPS Cu 2p core level photoemission spectra (PS) of the $CuO_{0.4}$ layer with and without irradiation. Considering the inelastic mean free path of photoelectrons whose kinetic energy is approximately 300 eV, information about copper valence states can be obtained within 0.8 nm [18] below the surface by the photoemission spectra. As can be seen in Figure 5, a broad shake-up satellite line due to the charge transfer [19,20] appeared in the binding energy (BE) region from 937 to 941 eV of PS for the unirradiated sample and decreased in intensity after irradiation. More quantitatively, the intensity ratio of the satellite to the main line at BE of 932.4 eV was 0.16 and 0.10 for the unirradiated and irradiated samples, respectively. These results indicate that the unirradiated sample included the copper valence state $Cu^{2+}$ and it was transformed into $Cu^+$ and/or $Cu^0$ ($Cu^+/Cu^0$) by irradiation. Thus the 5 keV-Ar$^+$ irradiation reduced $Cu^{2+}$ to $Cu^+/Cu^0$. The irradiation-induced reduction observed in the present work could be seen in the change in the shape of the Cu $2p_{3/2}$ lines before and after irradiation.

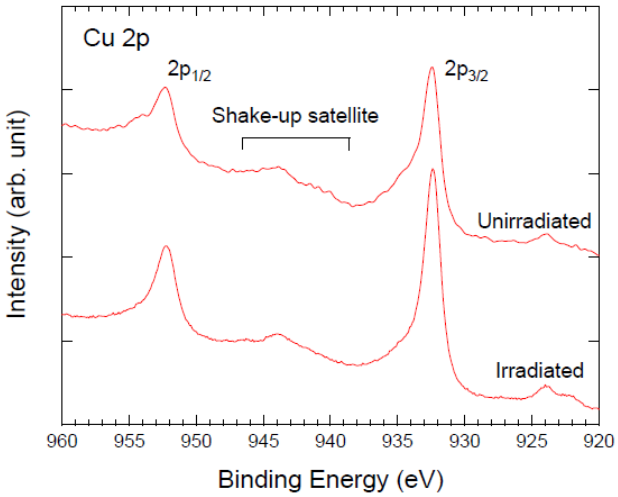


**Figure 5.** XPS Cu 2p core level photoemission spectra of the unirradiated and irradiated areas in the sample irradiated with 5 keV-$Ar^+$ ions to a fluence of $1 \times 10^{15}$ $cm^{-2}$.

Figure 6a,b depicts Cu $2p_{3/2}$ lines for the samples before and after irradiation, respectively. Each spectral line consists of three components denoted by I, II, and III. The lines, after background subtraction by the Shirly method [21], were decomposed by three Voigt functions using a curve fitting procedure. The component I located at BE of 932.4 eV was assigned to be Cu and/or $Cu_2O$. The BE of Cu (932.6 eV) [22–24] is very close to that of $Cu_2O$ (932.5 eV) [25–28], therefore the component I cannot be further decomposed by a curve fitting. The components II and III located at BE of 933.6 eV and 934.8 correspond to CuO [28–31] and $Cu(OH)_2$ [28,32], respectively. The fractions of each component obtained by the curve fitting are summarized in Table 1 for the samples with and without irradiation. The fractions corresponding to copper valence state $Cu^{2+}$ (CuO and $Cu(OH)_2$) decrease, while the fraction of $Cu^+/Cu^0$ ($Cu_2O$/Cu) increased by irradiation, indicating that the $Ar^+$ irradiation reduced $Cu^{2+}$ to $Cu^+/Cu^0$. This was consistent with the result deduced from the decrease in intensity of shake-up satellite line as described above.

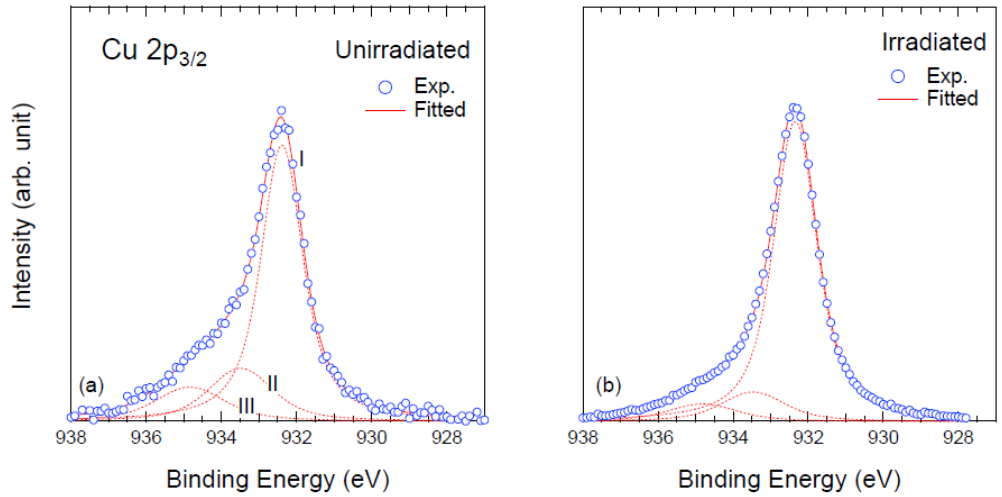


**Figure 6.** Detailed XPS Cu 2p3/2 core level photoemission spectra of the unirradiated (**a**) and irradiated (**b**) areas in the sample irradiated with 5 keV-$Ar^+$ ions to a fluence of $1 \times 10^{15}$ $cm^{-2}$. Each spectrum was decomposed into three components denoted by I, II, and III.

**Table 1.** Compositions of Cu, Cu2O, CuO and $Cu(OH)_2$ determined by Cu $2p_{3/2}$ photoemission spectra (PS) lines for the unirradiated and irradiated samples.

| Samples | Compositions (%) | | | |
|---|---|---|---|---|
| | **Cu** | **$Cu_2O$** | **CuO** | **$Cu(OH)_2$** |
| Unirradiated | 73.8 (65.7) [1] | (8.1) [1] | 16.5 | 9.7 |
| Irradiated | 94.1 (65.7) [1] | (28.4) [1] | 5.5 | 0.4 |

[1] These values were obtained by the assumption that the composition of the analyzing layer was $CuO_{0.4}$ before irradiation and the fraction of Cu was unchanged after irradiation.

The concentration ratio of $Cu_2O$ to Cu can be indirectly determined by the atomic ratio O/Cu of analyzing layer using the fractions of three components. Of course, the O/Cu can be calculated by the intensity ratio of O 1s to Cu 2p PS lines. However, it is impossible to accurately determine the atomic ratio O/Cu because of the presence of adventitious carbon contamination that includes oxygen atoms in the outermost layer. Therefore, the atomic ratio O/Cu in the analyzing layer was assumed to be 0.4 that was determined by RBS, resulting in the concentration ratio $Cu_2O$/Cu of 8.2/65.7 for the sample without irradiation. These values are presented with parenthesis in Table 1. For the sample with irradiation, the atomic ratio O/Cu in the analyzing layer was definitely different from that in the oxide layer, and thus, the composition $CuO_{0.38}$ determined by the combination of RBS and NRA could not be used to calculate the fraction of $Cu_2O$/Cu. Therefore, the fraction of metallic copper was assumed to be unchanged after irradiation. In fact, Panzner et al. [33] demonstrated that the oxide CuO was reduced to $Cu_2O$, while the oxide $Cu_2O$ was much more stable and no more reduction to Cu occurred under sputtering with 3–5 keV $Ar^+$ to a low fluence. Then the concentration ratio $Cu_2O$/Cu was calculated to be 28.4/65.7 for the sample with irradiation. These values were also presented inside parenthesis in Table 1.

As described above, XPS analysis revealed that the 5 keV-$Ar^+$ irradiation reduced $Cu^{2+}$ to $Cu^+/Cu^0$ in the cuprate. This result is consistent with the previous studies that CuO thin films were transformed into $Cu_2O$ by ion irradiation [33,34]. Next, the relationship between the reduction and the chromatic change was discussed briefly.

It is well known that the color of cuprous oxide ($Cu_2O$) powder is red. In addition, $Cu_2O$ in the form of both the thin film [35,36] and nanoparticle [37,38] would be reddish considering their optical absorption spectra. On the other hand, the color of the irradiated layer was found to be dark blue-purple, different from the color of pure $Cu_2O$. Fredj and Burleigh [39] showed that the color of a copper oxide layer in which $Cu_2O$ is primarily included varied from bare copper color to green depending on its thickness. Thus, they demonstrated the possibility that the $Cu_2O$ layer exhibited the color other than red. One possibility for the chromatic change is the presence of $Cu_2O$ phase in a metallic Cu phase. Another possibility is the change in a refractive index of the oxide layer accompanied by the change in chemical states of Cu and/or radiation damage by Ar ions. Unfortunately, the dominant effect on the chromatic change is unclear at present.

As mentioned in the Introduction, the beam spot in the sample irradiated with 5 keV-$Ar^+$ ions using the other machine turned bare copper color due to the removal of an oxide layer by sputtering, different from the present work. The reason for this difference is unknown but may result from the initial thickness and composition of the oxide layer. Further studies with various thicknesses and compositions are needed to clarify the mechanism underlying the irradiation-induced chromatic change in copper oxide layers. In addition, the minimum fluence at which the chromatic change can be recognized is necessary to examine for the applicability of the new type of a beam viewer. Such investigations are now in progress.

## 4. Conclusions

The color of a thin copper oxide layer formed on a copper plate turned from reddish-brown to dark blue-purple by irradiation with 5 keV $Ar^+$ ions to a fluence of $1 \times 10^{15}$ $Ar^+$ $cm^{-2}$. Nuclear reaction analysis revealed that a significant amount of oxygen ($5 \times 10^{15}$ O atoms·$cm^{-2}$) was released from the irradiated layer. The reduction of cupric oxide (CuO) to cuprous oxide ($Cu_2O$) occurred in the layer after the irradiation as confirmed by the decrease in intensity of a shake-up satellite line and the change in the shape of a Cu $2p_{3/2}$ line in photoemission spectra. The reduction led to the compositional change in the mixture of $Cu/Cu_2O/CuO$, which would result in the chromatic change.

**Author Contributions:** Conceptualization, K.T. and T.K.; methodology, K.T.; RBS and NRA, F.N.; data curation, T.K. and K.T.; writing—original draft preparation, K.T.; writing—review and editing, K.T. and T.K. All authors have read and agreed to the published version of the manuscript.

**Funding:** This research received no external funding.

**Conflicts of Interest:** The authors declare no conflict of interest.

## References

1. Peña-Rodríguez, O.; Crespillo, M.L.; Díaz-Nuñez, P.; Perlado, J.M.; Rivera, A.; Olivares, J. In situ monitoring the optical properties of dielectric materials during ion irradiation. *Opt. Mater. Express* **2016**, *6*, 734–742. [CrossRef]
2. Rivera, A.; Olivares, J.; Prada, A.; Crespillo, M.L.; Caturla, M.J.; Bringa, E.M.; Perlado, J.M.; Peña-Rodríguez, O. Permanent modifications in silica produced by ion-induced high electronic excitation: Experiments and atomistic simulations. *Sci. Rep.* **2017**, *7*, 10641. [CrossRef]
3. Zhou, J.; Li, B. Origins of a damage-induced green photoluminescence band in fused silica revealed by time-resolved photoluminescence spectroscopy. *Opt. Mater. Express* **2017**, *7*, 2888–2898. [CrossRef]
4. Crespillo, M.L.; Graham, J.T.; Zhang, Y.; Weber, W.J. In-situ luminescence monitoring of ion-induced damage evolution in $SiO_2$ and $Al_2O_3$. *J. Lumin.* **2016**, *172*, 208–218. [CrossRef]
5. Bandourko, V.; Umeda, N.; Plaksin, O.; Kishimoto, N. Heavy-ion-induced luminescence of amorphous $SiO_2$ during nanoparticle formation. *Nucl. Instrum. Meth. B* **2005**, *230*, 471–475. [CrossRef]
6. Forck, P.; Andre, C.; Becker, F.; Haseitl, R.; Reiter, A.; Walasek-Höhne, B.; Krishnakumar, R.; Ensinger, W. Scintillation Screen Investigations for High Energy Heavy Ion Beams at GSI. In Proceedings of the DIPAC2011, Hamburg, Germany, 16–18 May 2011; pp. 170–172.
7. Johnson, C.D. *The Development and Use of Alumina Ceramic Fluorescent*; CERN/PS/90-12(AR); European Laboratory for Particle Physics: Geneva, Switzerland, 1990.
8. Takahiro, K.; Terai, A.; Kawatsura, K.; Naramoto, H.; Yamam, S.; Tsuchiya, B.; Nagata, S.; Nishiyama, F. Rutherford backscattering spectrometry of electrically charged targets: Elegant technique for measuring charge-state distribution of backscattered Ions. *Jpn. J. Appl. Phys.* **2006**, *45*, 1823–1825. [CrossRef]
9. Parajuli, R.K.; Kada, W.; Kawabata, S.; Matsubara, Y.; Sakai, M.; Miura, K.; Satoh, T.; Koka, M.; Yamada, N.; Kamiya, T.; et al. Ion-Beam-Induced Luminescence Analysis of β-SiAlON:Eu Scintillator under Focused Microbeam Irradiation. *Sens. Mater.* **2016**, *28*, 837–844.
10. Warren, A.J.; Thomas, C.B.; Reehal, H.S.; Stevens, P.R.C. A study of the luminescent and electrical characteristics of films of ZnS doped with Mn. *J. Lumin.* **1983**, *28*, 147–162. [CrossRef]
11. Calusi, S.; Colombo, E.; Giuntini, L.; Giudice, A.L.; Manfredotti, C.; Massi, M.; Pratesi, G.; Vittone, E. The ionoluminescence apparatus at the LABEC external microbeam facility. *Nucl. Instrum. Meth. B* **2008**, *266*, 2306–2310. [CrossRef]
12. Feldmann, C.; Jüstel, T.; Ronda, C.R.; Schmidt, P.J. Inorganic Luminescent Materials: 100 Years of Research and Application. *Adv. Funct. Mater.* **2003**, *13*, 511–516. [CrossRef]
13. Kleiman, J.; Iskanderova, Z.; Best, C.; Dennison, J.R.; Wood, B. Long-term stability of ion-beam treated space polymers in geo-simulated environment. In Proceeding of the 14th ISMSE $ 12th ICPMSE, Biarritz, France, 1–5 October 2018.
14. Plis, E.A.; Engelhart, D.P.; Cooper, R.; Johnston, W.R.; Ferguson, D.; Hoffmann, R. Review of Radiation-Induced Effects in Polyimide. *Appl. Sci.* **2019**, *9*, 1999. [CrossRef]
15. Matienzo, L.J.; Emmi, F.; Van Hart, D.C.; Gall, T.P. Interactions of high-energy ion beams with polyimide films. *J. Vac. Sci. Technol. A* **1989**, *7*, 1784–1789. [CrossRef]
16. Computer Simulation of RBS, ERDA, NRA, MEIS and PIGE by Matej Mayer. Available online: https://home.mpcdf.mpg.de/~{}mam/Version6.html (accessed on 5 December 2020).
17. Ziegler, J.F.; Ziegler, M.D.; Biersack, J.P. SRIM—The stopping and range of ions in matter (2010). *Nucl. Instrum. Meth. B* **2010**, *268*, 1818–1823. [CrossRef]
18. Tanuma, S.; Powell, C.J.; Penn, D.R. Calculations of electron inelastic mean free paths. II. Data for 27 elements over the 50–2000 eV range. *Surf. Interface Anal.* **1991**, *17*, 911–926. [CrossRef]

19. Kawai, J.; Tsuboyama, S.; Ishizu, K.; Miyamura, K.; Saburi, M. Covalency of copper complex determined by Cu 2p X-ray photoelectron spectrometry. *Anal. Sci.* **1991**, *7*, 337–340. [CrossRef]
20. Pawar, S.M.; Kim, J.; Inamdar, A.I.; Woo, H.; Jo, Y.; Pawar, B.S.; Cho, S.; Kim, H.; Im, H. Multi-functional reactively-sputtered copper oxide electrodes for supercapacitor and electro-catalyst in direct methanol fuel cell applications. *Sci. Rep.* **2016**, *6*, 21310. [CrossRef] [PubMed]
21. Végh, J. The Shirley background revised. *J. Electron Spectrosc. Relat. Phenom.* **2006**, *151*, 159–164. [CrossRef]
22. Anderson, C.R.; Lee, R.N. Comparison of APS and FRESCA core level binding energy measurements. *J. Vac. Sci. Technol.* **1982**, *20*, 617–621. [CrossRef]
23. Seah, M.P.; Gilmore, I.S.; Beamson, G. XPS: Binding energy calibration of electron spectrometers 5—re-evaluation of the reference energies. *Surf. Interface Anal.* **1998**, *26*, 642–649. [CrossRef]
24. Bird, R.J.; Swift, P. Energy calibration in electron spectroscopy and the re-determination of some reference electron binding energies. *J. Electron Spectrosc. Relat. Phenom.* **1980**, *21*, 227–240. [CrossRef]
25. McIntyre, N.S.; Cook, M.G. X-ray photoelectron studies on some oxides and hydroxides of cobalt, nickel, and copper. *Anal. Chem.* **1975**, *47*, 2208–2213. [CrossRef]
26. Schön, G. ESCA studies of Cu, Cu2O and CuO. *Surf. Sci.* **1973**, *35*, 96–108. [CrossRef]
27. Losev, A.; Rostov, K.; Tyuliev, G. Electron beam induced reduction of CuO in the presence of a surface carbonaceous layer: An XPS/HREELS study. *Surf. Sci.* **1989**, *213*, 564–579. [CrossRef]
28. Deroubaix, G.; Marcus, P. X-ray photoelectron spectroscopy analysis of copper and zinc oxides and sulphides. *Surf. Interface Anal.* **1992**, *18*, 39–46. [CrossRef]
29. Haber, J.; Machej, T.; Ungier, L.; Ziółkowski, J. ESCA studies of copper oxides and copper molybdates. *J. Solid State Chem.* **1978**, *25*, 207–218. [CrossRef]
30. Gaarenstroom, S.M.; Winograd, N. ESCA spectra of cadmium and silver oxides. *J. Chem. Phys.* **1977**, *67*, 3500–3506. [CrossRef]
31. Tobin, J.P.; Hirschwald, W.; Cunningham, J. XPS and XAES studies of transient enhancement of $Cu^1$ at CuO surfaces during vacuum outgassing. *Appl. Surf. Sci.* **1983**, *16*, 441–452. [CrossRef]
32. Biesinger, M.C. Advanced analysis of copper X-ray photoelectron spectra. *Surf. Interface Anal.* **2017**, *49*, 1325–1334. [CrossRef]
33. Panzner, G.; Egert, B.; Schmidt, H.P. The stability of CuO and $Cu_2O$ surfaces during argon sputtering studied by XPS and AES. *Surf. Sci.* **1985**, *151*, 400–408. [CrossRef]
34. Dementyeva, M.M.; Prikhodko, K.E.; Gurovich, B.A.; Bukina, Z.V.; Komarov, D.A.; Kutuzov, L.V. Phase transitions in copper oxide thin films under proton irradiation. *IOP Conf. Ser. Mater. Sci. Tecnol.* **2017**, *256*, 012020. [CrossRef]
35. Pan, J.; Yang, C.; Gao, Y. Investigations of Cuprous Oxide and Cupric Oxide Thin Films by Controlling the Deposition Atmosphere in the Reactive Sputtering Method. *Sens. Mater.* **2016**, *28*, 817–824.
36. Gevorkyan, V.A.; Reymers, A.E.; Nersesyan, M.N.; Arzakantsyan, A.M. Characterization of $Cu_2O$ thin films prepared by evaporation of CuO powder. *J. Phys. Conf. Ser.* **2012**, *350*, 012027. [CrossRef]
37. Goua, L.; Murphy, C.J. Controlling the size of $Cu_2O$ nanocubes from 200 to 25 nm. *J. Mater. Chem.* **2004**, *14*, 735–738. [CrossRef]
38. Butte, S.M.; Waghuley, S.A. Optical properties of $Cu_2O$ and CuO. *AIP Conf. Proc.* **2020**, *2220*, 020093.
39. Fredj, N.; Burleigh, T.D. Transpassive Dissolution of Copper and Rapid Formation of Brilliant Colored Copper Oxide Films. *J. Electrochem. Soc.* **2011**, *158*, C104–C110. [CrossRef]